Human Papilloma Virus DNA Detection in Clinical Samples Using Fluorogenic Probes Based on Oligonucleotide Gated Nanoporous Anodic Alumina Films

Andy Hernández-Montoto, M. Nieves Aranda, Isabel Caballos, Alba López-Palacios, María Ángeles Tormo-Mas, Javier Pemán, Mireya Prieto Rodríguez, Carlos Picornell, Elena Aznar,* and Ramón Martínez-Máñez*

In this work, fluorogenic probes based on oligonucleotide capped nanoporous anodic alumina films are developed for specific and sensitive detection of human papilloma virus (HPV) DNA. The probe consists of anodic alumina nanoporous films loaded with the fluorophore rhodamine B (RhB) and capped with oligonucleotides bearing specific base sequences complementary to genetic material of different high-risk (hr) HPV types. Synthesis protocol is optimized for scale up production of sensors with high reproducibility. The sensors' surfaces are characterized by scanning electron microscopy (HR-FESEM) and atomic force microscopy (AFM) and their atomic composition is determined by energy dispersive X-ray spectroscopy (EDXS). Oligonucleotide molecules onto nanoporous films block the pores and avoid diffusion of RhB to the liquid phase. Pore opening is produced when specific DNA of HPV is present in the medium, resulting in RhB delivery, that is detected by fluorescence measurements. The sensing assay is optimized for reliable fluorescence signal reading. Nine different sensors are synthesized for specific detection of 14 different hr-HPV types in clinical samples with very high sensitivity (100%) and high selectivity (93–100%), allowing rapid screening of virus infections with very high negative predictive values (100%).

1. Introduction

Infectious diseases represent one of the most important health problems causing ≈15 million deaths annually worldwide. In this context, the development of new systems for rapid detection of pathogens is of relevance for the advance in early diagnosis, finding appropriate treatments, a much more favorable patients' recovery, a reduction in associated mortality, and a significant economic saving. Among infectious diseases, human papilloma virus infection is one of the most important caused by viruses.[1,2,3] Human papilloma virus (HPV) belongs to the *Papillomaviridae* family, infecting and replicating in the nucleus of epithelial cells.[4,5] It has a simple structure formed by a protein capsid without envelope and the genetic material (circular double stranded DNA: ≈8000 base pairs) that lies in its interior.[6,7,8] Based on their

A. Hernández-Montoto, M. N. Aranda, I. Caballos, A. López-Palacios,
E. Aznar, R. Martínez-Máñez
The Inter-University Research Institute for Molecular Recognition and
Technological Development
Technical University of Valencia
University of Valencia
Camino de Vera s/n, Valencia 46022, Spain
E-mail: elazgi@upvnet.upv.es; rmaez@qim.upv.es
A. Hernández-Montoto, E. Aznar, R. Martínez-Máñez
CIBER Bioengineering, Biomaterials and Nanomedicine
Carlos III Health Institute
Avenida Monforte de Lemos 3-5, Madrid 28029, Spain

A. Hernández-Montoto, M. N. Aranda, I. Caballos, A. López-Palacios,
E. Aznar, R. Martínez-Máñez
Joint Research Unit in Nanomedicine and Sensors
Health Research Institute Hospital La Fe
Technical University of Valencia
Avenida Fernando Abril Martorell 106, Valencia 46026, Spain
M. Á. Tormo-Mas, J. Pemán
Accredited Research Group on Serious Infection
Health Research Institute Hospital La Fe
Avenida Fernando Abril Martorell 106, Valencia 46026, Spain
J. Pemán
Microbiology Service
Polytechnic and University Hospital La Fe
Avenida Fernando Abril Martorell 106, Valencia 46026, Spain
M. P. Rodríguez
Pathological Anatomy Service
Polytechnic and University Hospital La Fe
Avenida Fernando Abril Martorell 106, Valencia 46026, Spain
C. Picornell
Arafarma Group
C/ Fray Gabriel de San Antonio, 6–10, Marchamalo 19180, Guadalajara,
Spain
E. Aznar, R. Martínez-Máñez
UPV-CIPF Joint Research Unit in Mechanisms of Diseases and
Nanomedicine
Valencia
Technical University of Valencia
València 46012, Spain

DNA composition (difference of more than 10% in the nucleotide sequences in the E6, E7, and L1 region) ≈77 HPV genotypes have been described. Specific types are considered as high risk (hr) HPV types because they have been identified as causative agents of cervical cancer.[9,10,11] Therefore, screening tools to detect hr-HPV infection allow cervical cancer prevention, management, and treatment.[12,13,14] Moreover, hr-HPV testing on cervical samples appeared to be more sensitive for the detection of cervical intraepithelial neoplasia grade 2 or worse (CIN2+) than cytology, though often less specific.[15,16] In this regard, many testing assays have been used for the detection of a broad spectrum of hr-HPV types with high reliability, reproducibility, and accuracy.[17,18,19] They include assays that can detect DNA-RNA hybrids without genotyping like the Hybrid Capture 2 (HC2) HPV DNA test, approved by the FDA in 2003, and PCR based assays that can detect HPV DNA with partial genotyping of hr-HPV, like the Cobas 4800 HPV test, approved by the FDA in 2011.[20] These assays have a high sensitivity and negative predictive values. However, they have some drawbacks such as a relatively lower specificity and positive predictive values and the use of expensive, time consuming, and complex methods requiring trained personnel. Therefore, alternative rapid diagnostic platforms for the detection of different hr-HPV types using smart nanodevice-based biosensors have been designed and developed.[21,22,23] These materials include different types of nanoparticles and electrodes whose surfaces have been modified with different oligonucleotide probes for specific recognition of target DNA.[24,25,26] In these systems, the transduction leading to measurable signal are mainly based on optical and electrochemical processes.[27,28,29] Nevertheless, these reported sensors have been designed only for detection of a few hr-HPV types (mainly 16 and 18) and their capacity for direct HPV detection in clinical samples (detection without any sample treatment) is not usually tested or validated.

The design and development of smart nanodevice-based biosensors bearing gated porous supports for detection of different DNA of pathogens have received increasing attention during the last years.[30,31,32] These hybrid materials are mainly composed of two subunits: an inorganic porous support in which a fluorogenic molecule can be loaded and a molecular or supramolecular entity grafted onto external surface that can control the fluorophore probe diffusion from inside the pore to the liquid phase.[33,34,35] In these examples, capping molecules on the support's surface act as molecular gates (also known as gate-keepers) blocking the pores and avoiding dye release. Only when specific stimuli are present, as for instance a target analyte to be detected, the structural state of molecular gates changes, unblocking the pores and leading to controlled dye delivery which can be measured by fluorescence spectroscopy.[36] Specifically, in gated biosensors based on this paradigm, a fluorescent signal in the medium is related to the presence of specific genetic material of pathogens, due to the transduction process triggered by the recognition between pathogen's DNA molecules in the medium and a gating oligonucleotides on the porous support's surface, that finally enables the release of the loaded fluorophore.[37] Among inorganic porous supports, mesoporous silica nanoparticles[38,39] and nanoporous anodic alumina (NAA) films[40,41] have been used for sensor development because they have an ordered porous structure composed of tailor-made pores with large specific surface area and pore volume. These supports have high loading capacity and their external surface can be easily modified with alkoxysilane chemistries bearing different functional groups to yield an organic/inorganic interphase, enabling further functionalization of support's surface with additional molecules or supramolecules through physical interactions or chemical linkages.[42,43] In this regard, nanoporous anodic alumina-based electrochemical biosensors have been used recently for sensitive detection of different analytes including DNA biomolecules.[44,45,46]

Different oligonucleotide-gated porous based sensors have been reported for detection of DNA/RNA or antigens of different pathogens such as: *Mycoplasma*,[30,31,47] *Candida albicans*,[32] *Candida auris*,[48] *Staphylococcus aureus*,[49] *Pneumocystis jirovecii*,[50] and SARS-CoV-2 virus.[51] These systems are currently demonstrating great potential for the development of sensitive, selective, and low-cost biosensors. However, similar biosensors for detection of hr-HPV types have not been reported yet. In this work sensors for detection of HPV were developed. Specifically, the platform is configured for the rapid detection of 14 different hr-HPV types associated with the appearance of cervical cancer. For that, a set of 9 biomaterials based on NAA films coated with nucleic acid molecules as gates were designed. The probes consisted of nanoporous anodic alumina supports loaded with rhodamine B (RhB) and whose pores were blocked with diverse oligonucleotide sequences that specifically recognize HPV types (**Figure 1**). The release of the dye from the prepared materials is tested in the presence of the complementary oligonucleotide and validated in clinical samples, demonstrating the potential of this approach for multiplexed screening of HPV infections.

2. Results and Discussion

Schematic representations of the developed sensors and the steps to prepare them are shown in Figure 1 and **Figure 2**, respectively, whereas the sequences of the oligonucleotides used for the preparation of the sensors are listed in **Table 1**. Capping oligonucleotides **O2-S1-9** have the DNA base sequence of different HPV types overall being able to recognize 14 HPV types, whereas target oligonucleotides **O3-S1C-9C** are the corresponding complementary oligonucleotides used in optimization and testing assays (vide infra). The NAA supports are commercially available and have an alumina thickness of 10 ± 0.2 µm, a pore diameter of 5 ± 2 nm and a pore density of 9×10^{11} cm^{-2}.

The starting NAA porous support (**D0**) was easily loaded with the RhB fluorophore by soaking NAA disks in a RhB solution in acetonitrile and gently stirring with an orbital stirrer, yielding **D1**. High loaded dye content was achieved using highly concentrated RhB solution in short times of interaction between both phases. RhB encapsulation was evidenced by EDXS analysis. The C, N, and O atomic content in the dye-loaded NAA disk slightly increases with respect to the unmodified support. Note that the X-ray emission depth for analyzed atoms (<100 nm at 5 kV) is lower than the NAA film thickness (10 µm). (**Figure 3**, **Table 2**; Figure S1 and Tables S1,S2 (Supporting Information)).

After dye loading, the external surface of the NAA support was functionalized with isocyanate groups to yield **D2** through the reaction between Al-OH groups at the external surface with 3-(triethoxysilyl)propyl isocyanate, resulting in the formation of Al-O-Si bonds (Figure 2). In this step, NAA disks were placed on the bottom surface of a closed flask ensuring that NAA films are

Table 1. Nucleotide sequences of 19 oligonucleotides used for sensor preparation and sensing assay.

Oligonucleotide	hr-HPV type	Nucleotide sequence 5'-....-3'
O1	-	NH$_2$-(CH$_2$)$_6$-AAA AAA CCC CCC
O2-S1	59, 16, 18	TTTTGGGGGAGACTGACAAATATCCAATGCTACTTCACTTTTGTTATCCTGCAACAATTTAAGGGGGGTTTT
O3-S1C	59, 16, 18	TTAAATTGTTGCAGGATAACAAAAGTGAAGTACCCATTGGATATTTGTCAGTCT
O2-S2	45, 18	TTTTGGGGGGTTTTGTCAATCAGTTGCTTGTTACCTGTCAAAAGGATACTACACCTCCAGAAAAGCACGGATCCATATGATAAATTAAAGTGGGGGGTTTT
O3-S2C	45, 18	ACTTTAATTTATCATATGCGATCCTGCTTTTCTGGAGGTGTAGTATCCTTTGACAGGTAACACAGCAACTGATTGCACAAAC
O2-S3	31, 16	TTTTGGGGGTAGCTAAAGTAGCTGTTGAACCGAGCCTTTAATATAAGTCAGTAGGGACCGATTCACCAACCGTGCCTGAGGGGGGTTTT
O3-S3C	31, 16	TCAGGCACCGTTGGTGAATCCGTCCCTACTGACTTATATATTAAAGGCTCCGTTCAACAGCTACTTTAGCTA
O2-S4	51	TTTTGGGGGCTTGTAGGTGTTGGGAAGACATTCCTAACGATTATTATTATTAAGGGGGGGTTTT
O3-S4C	51	CCTTAATATAATAATCGTTAGGAATGTCTTCCCCAACACCTACAAG
O2-S5	52	TTTTGGGGGGCCTTTATTAAAACAAGTTTGATGATACTGAAACCAGTAACAAATGCTGGTAAACCTGGTATAGATAATAGGGAATGTTGGGGGGTTTT
O3-S5C	52	AACATTCCCTATTATCTATACCAGGTTTACCAGCATATTTGTTACTGGCATTGTAGCGTTGAAATAGGTAGAGGGCAGCCATTAGGCGTTGGCATAAGTGGTGGGGGGTTTT
O2-S6	33, 58	TTTTGGGGGGACCCTGATACACAACGATTAGTATGGGCATTTGTAGGCCTTGAAATAGGTAGAGGGCAGCCATTAGGCGTTGGCATAAGTGGTGGGGGGTTTT
O3-S6C	33, 58	ACCACTTATGCCAACGCCTAATGGCTGCCCTCTACCTATTTCAAGGCTACACATGCCCATACTAATCGTTGTGTATCAGGGT
O2-S7	35, 33	TTTTGGGGGGGCCTTAAAATTCCTTAAAATTGTCATTTTATATGTACTGTCACTACAGAAGACACAGCAGACACATATTTGTACTACCGGGTTGGGGGGGTTTT
O3-S7C	35, 33	AACCCGTAGTACAAATATGTCTGTGTTCTGTCGTCTTCTTCAGTGACAGTACATATAAAAATGACAATTTTAAGGAATATTTAAGGC
O2-S8	56, 66	TTTTGGGGGGGGTACTGATTAATTTTTCGTGCATCATATTTACTTAACTGTTCTGTAGCAGTACTAATAGTCGGGGGGTTTT
O3-S8C	56, 66	GACTATTAGTACTGCTACAGAACAGTTAAGTAAATATGATGCACGAAAAATTAATCAGTACC
O2-S9	68, 39	TTTTGGGGGGGGACTGTCACGTATGCTCAGTGCCCTAATATAACAATTCAGTAGGTATAGTGTCCCCTACCATGCCCGGGGGTTTT
O3-S9C	68, 39	GGCATGGTAGGGACGACTATACCTACTGAATTGTATATTAAGGGCACTGACATACGTGACAGTCC

2203326 (3 of 13)

**ADVANCED
SCIENCE NEWS**

www.advancedsciencenews.com

**ADVANCED
HEALTHCARE
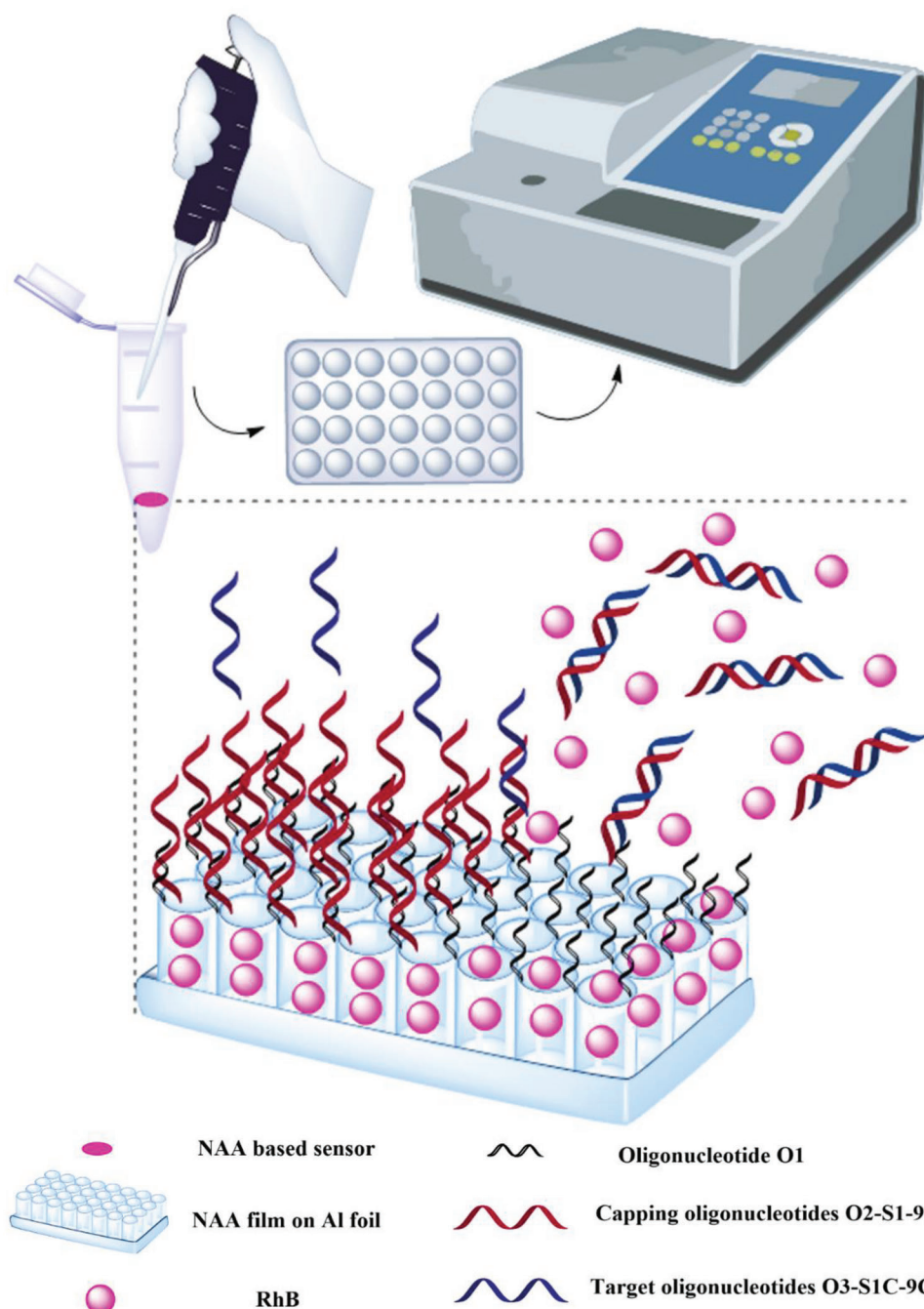MATERIALS**

www.advhealthmat.de

Figure 1. Scheme of fluorogenic sensors for HPV DNA detection based on oligonucleotide gated NAA films loaded with rhodamine B.

side up oriented, allowing a better interaction between the alumina surface with the species dissolved in the liquid phase. Also, a gentle mixing with an orbital stirrer ensures more homogenous conditions for surface functionalization allowing to obtain sensors in a reproducible manner. Humidity control is also important during these steps to avoid isocyanate hydrolysis and allow a controlled coupling between Al-OH groups at the external surface with 3-(triethoxysilyl)propyl isocyanate, also avoiding uncontrolled alkoxysilane hydrolysis and condensation to form a solid phase on the external surface of the sensors. To avoid humidity, it

is important to use freshly prepared RhB solutions for the synthesis and washing steps and use a tightly closed reaction flask. The surface's functionalization with the alkoxysilane was evidenced by electron microscopy and EDXS analysis. Si, C, and N atomic content increase after surface modification (Figure 3, Table 2 and Figure S1, Table S3, Supporting Information).

Isocyanate-modified NAA supports (**D2**) were functionalized with oligonucleotide **O1**, bearing and amine group, through urea linkages, to yield **D3**. The oligonucleotide base sequence in **O1** allows the further hybridization of the capping oligonucleotides

**ADVANCED
SCIENCE NEWS**

www.advancedsciencenews.com

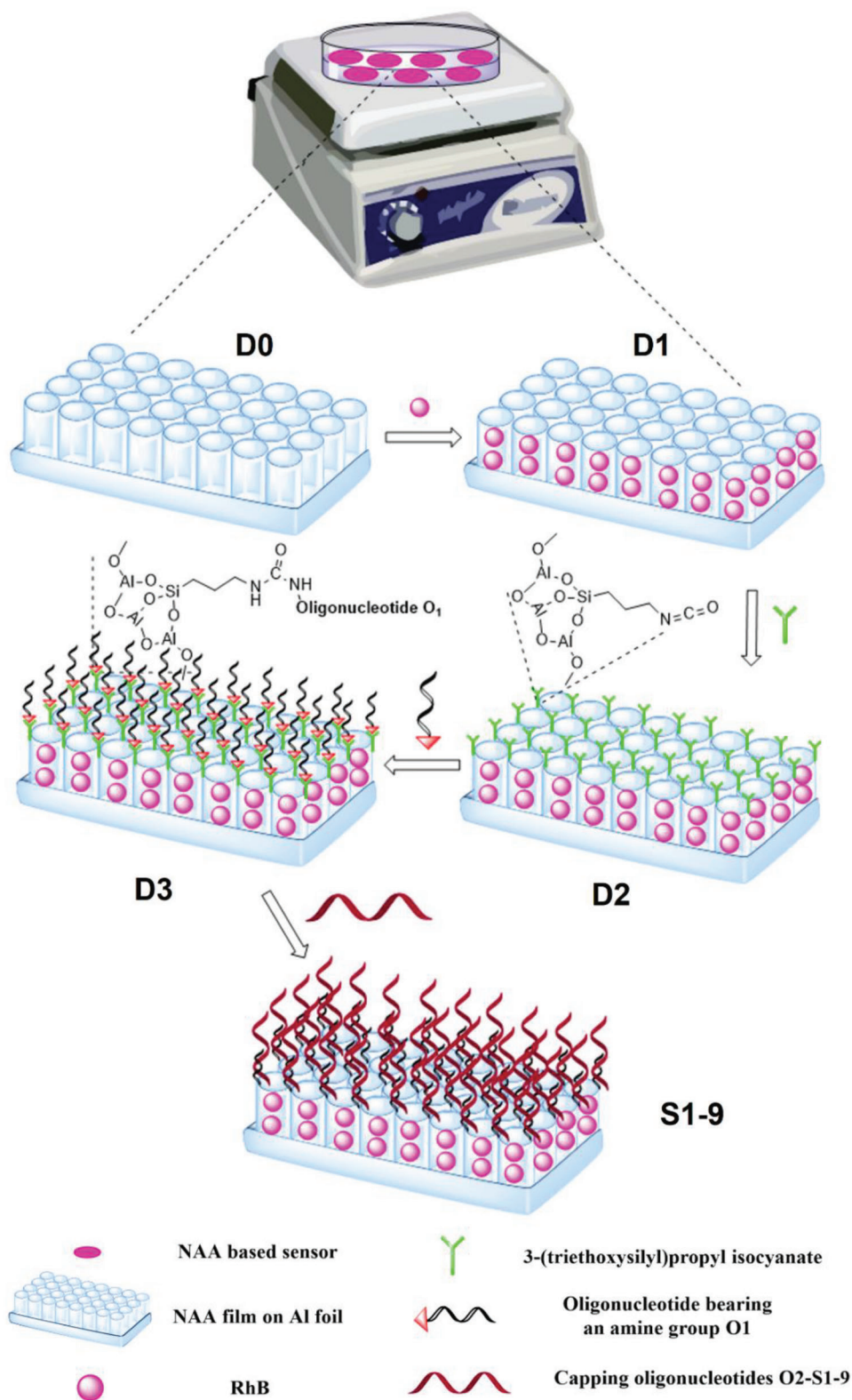**ADVANCED
HEALTHCARE
MATERIALS**

www.advhealthmat.de

Figure 2. Scheme of the synthesis steps of fluorogenic sensors (**S1-9**) for HPV DNA detection based on oligonucleotide gated NAA films loaded with rhodamine B.
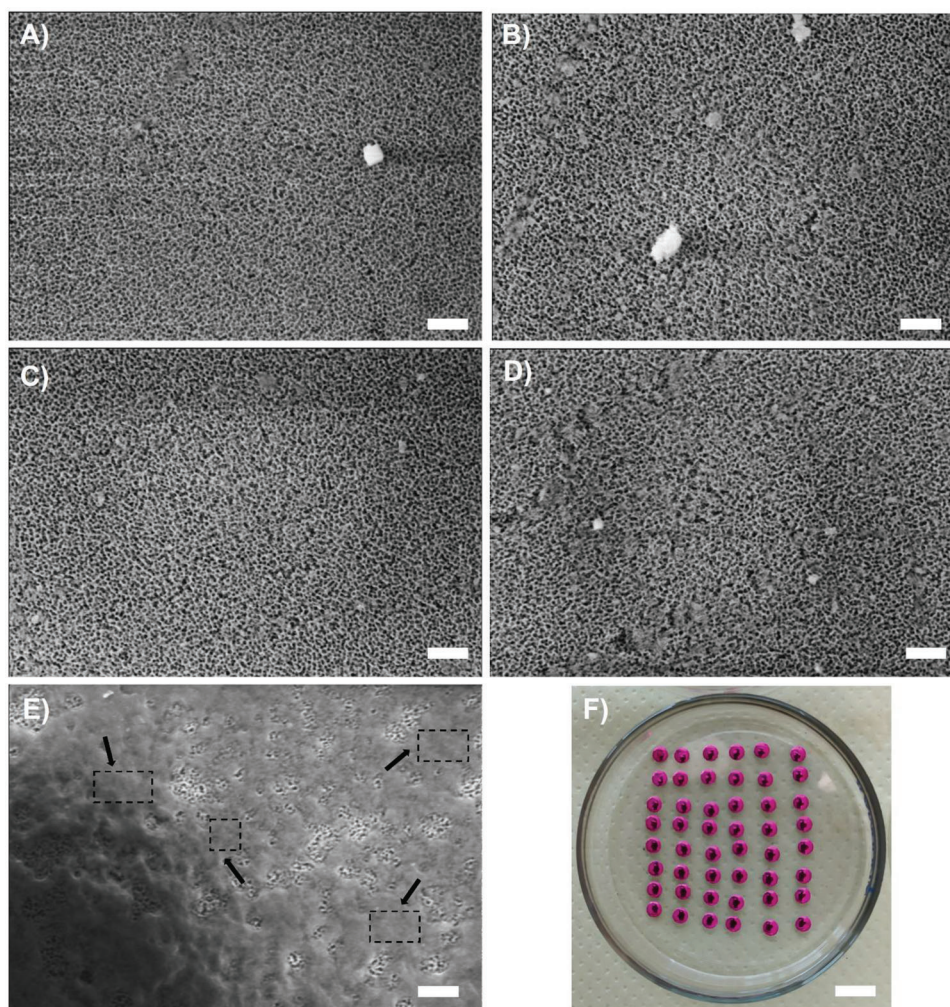
Figure 3. HR-FESEM images of NAA surfaces during synthesis steps (**D0** A); **D1** B); **D2** C); **D3** D), and final sensors **S1-9** E), (scale bars: 200 nm) and photographs of the final NAA based sensors F) (Scale bar: 1 cm). Black arrows indicate some surface areas of porous alumina films coated with a thin layer of gating oligonucleotides.

Table 2. Relative atomic compositions respect to Al atoms of D0, D1, D2, and D3 by EDXS analysis.

Element	D0	D1	D2	D3
C	0.32 ± 0.01	0.49 ± 0.01	0.51 ± 0.02	0.59 ± 0.02
N	0	0.005 ± 0.002	0.042 ± 0.005	0.056 ± 0.006
O	2.31 ± 0.04	2.43 ± 0.03	2.29 ± 0.06	2.35 ± 0.06
Al	1.00 ± 0.02	1.00 ± 0.01	1.00 ± 0.03	1.00 ± 0.03
Si	0	0	0.037 ± 0.004	0.036 ± 0.004
P	0	0	0	0.006 ± 0.004

(**O2-S1-9**) containing the DNA base sequence of different HPV types (vide infra>) (Table 1). After the modification process, P, C, N, and O atomic content increases confirming oligonucleotide coupling to the NAA surface (Table 2). Lower values of atomic contents were obtained when a higher volume of more diluted solution of oligonucleotide **O1** (10 µM, 600 µL) was used in the func-

tionalization process, indicating a lower surface coverage with the oligonucleotide (Table S4, Supporting Information). We also found that water content in the reaction mixture produces the hydrolysis of isocyanate groups on NAA surface that avoids the covalent coupling of oligonucleotide **O1** on NAA surface.

Finally, NAA disks were coated with oligonucleotides **O2-S1-9** containing the DNA base sequence of 14 different HPV types (part of the L1 region of their genomes coding the major capsid protein[9]) to yield sensors **S1-9**. These capping oligonucleotides contain in their extremes two sequences complementary to oligonucleotides **O1** (Table 1). Elimination of non-hybridized capping oligonucleotides **O2-S1-9** and RhB after the functionalization process, was confirmed by measuring the absorbance and fluorescence intensity of supernatants after washing. Both, absorbance at 260 nm corresponding to oligonucleotides **O2-S1-9**, and fluorescence intensity at 585 nm (λ_{ex} = 555 nm) corresponding to RhB, decreased after washing (Figure S2, Supporting Information). Following this protocol 9 sensors were obtained. All final NAA based sensors were also characterized

Table 3. Relative atomic compositions respect to Al atoms of the sensors S1-9 by EDXS analysis.

Element	S1	S2	S3	S4	S5	S6	S7	S8	S9
C	0.49 ± 0.01	0.77 ± 0.02	0.83 ± 0.02	0.94 ± 0.02	0.78 ± 0.02	1.18 ± 0.03	0.62 ± 0.02	1.14 ± 0.03	1.06 ± 0.03
N	0.028 ± 0.003	0.117 ± 0.006	0.143 ± 0.006	0.165 ± 0.007	0.145 ± 0.007	0.246 ± 0.009	0.107 ± 0.007	0.210 ± 0.008	0.141 ± 0.007
O	2.46 ± 0.04	2.52 ± 0.05	2.61 ± 0.05	2.64 ± 0.05	2.29 ± 0.05	2.73 ± 0.06	2.19 ± 0.06	2.88 ± 0.06	2.71 ± 0.06
Al	1.00 ± 0.02	1.00 ± 0.02	1.00 ± 0.02	1.00 ± 0.02	1.00 ± 0.02	1.00 ± 0.02	1.00 ± 0.03	1.00 ± 0.02	1.00 ± 0.02
Si	0.015 ± 0.002	0.077 ± 0.004	0.043 ± 0.003	0.032 ± 0.003	0.064 ± 0.004	0.045 ± 0.003	0.018 ± 0.003	0.052 ± 0.004	0.030 ± 0.003
P	0.010 ± 0.002	0.016 ± 0.003	0.036 ± 0.003	0.041 ± 0.004	0.030 ± 0.004	0.062 ± 0.005	0.039 ± 0.005	0.053 ± 0.005	0.038 ± 0.004

by electron microscopy and EDXS analysis (Figure 3, **Table 3**; Figure S1 and Tables S5–S13, Supporting Information). Oligonucleotides **O2-S1-9** have a tridimensional structure with nanometric dimensions and adopt a spatial arrangement on the alumina surface that blocked the pores and avoid the diffusion of the fluorophore from the porous structure of the material (vide infra). From a macroscopic point of view, oligonucleotide molecules form an organic layer on the inorganic porous support that can be seen in the electron microscopy images. Furthermore, P, C, N, and O atomic content increases after surface coating. This inorganic/organic interphase act as a physical barrier that control the diffusion of fluorophore between the porous solid support and the liquid medium. The presence of target complementary oligonucleotides in the medium hybridize to the gating oligonucleotides inducing a displacement, unblocking the pores, and the release of the entrapped fluorophore (vide infra). Finally, the surface morphology of alumina films during synthesis steps was also characterized by atomic force microscopy (Figure S3, Supporting Information).

After the synthesis and characterization of the 9 sensors, their capacity to selectively release RhB in the presence of oligonucleotides complementary to those used for capping was evaluated. Thus, NAA-based sensors were incubated with the corresponding complementary oligonucleotides **O3-S1C-9C** (Table 1) in TRIS buffer and released rhodamine B was measured by fluorescence spectroscopy at 585 nm (λ_{ex} = 555 nm) using a plate reader. NAA sensors disks (**S1-9**) non incubated with oligonucleotides were used as negative controls. The release profiles of RhB from the sensors are shown in **Figure 4**. The RhB release profile is plotted as fluorescence intensity variations at different times with respect to the initial intensity (I_t-I_0). Results are represented as means and standard deviations of measurements for 3 different nanodevices incubated with Tris (black squares) and other 3 nanodevices incubated with the corresponding complementary oligonucleotide (red circles). Data of individual nanodevices for all 9 developed sensors, are also shown in Figure S4 (Supporting Information). A negligible release of RhB was produced from sensors used as negative controls even at longer times (60 min), confirming the gating capacity of the oligonucleotides on the NNA surface that block the pores and avoid dye diffusion. In contrast, a remarkable dye release was found from NAA disks incubated with corresponding complementary oligonucleotides **O3-S1C-9C**. The complementary oligonucleotides hybridize with the capping oligonucleotides **O2-S1-9** on NAA surface, unblocking the pores, and finally leading to diffusion of RhB (Figure 1). Moreover, the calibration curves of the 9 sensors for the detection of the corresponding complementary

Table 4. Corresponding atomic composition and atomic ratios respect to Al atoms of NAA surfaces after sensing assay for control (A) and sensor S1 incubated with complementary oligonucleotides O3-S1C (B) by EDXS analysis.

A) Element	Wt.%	Atomic %	X/Al
C	11.2 ± 0.2	17.2 ± 0.3	0.68 ± 0.02
N	1.6 ± 0.1	2.1 ± 0.2	0.082 ± 0.007
O	45.5 ± 0.1	52.4 ± 0.5	2.08 ± 0.04
Al	37.0 ± 0.1	25.2 ± 0.3	1.00 ± 0.02
Si	4.33 ± 0.05	2.85 ± 0.05	0.113 ± 0.003
P	0.44 ± 0.03	0.26 ± 0.02	0.0103 ± 0.0009

B) Element	Wt.%	Atomic %	X/Al
C	8.9 ± 0.2	14.0 ± 0.3	0.51 ± 0.02
N	1.4 ± 0.1	1.9 ± 0.2	0.070 ± 0.007
O	45.5 ± 0.1	53.5 ± 0.5	1.95 ± 0.04
Al	39.4 ± 0.1	27.4 ± 0.3	1.00 ± 0.02
Si	4.36 ± 0.05	2.93 ± 0.05	0.107 ± 0.003
P	0.41 ± 0.03	0.25 ± 0.02	0.0091 ± 0.0008

oligonucleotides **O3-S1C-9C** are shown in Figure S5 (Supporting Information). The limit of detection (**LOD** = 92–265 pM) and sensitivity ($\Delta(I_{15}$-$I_0)/\Delta(\log c, M)$ = 300–2400) derived from the calibration curves are summarized in Table S14 (Supporting Information). These results confirm the potential capacity of these materials for rapid and sensitive detection of oligonucleotides containing the DNA base sequences of 14 different types of HPV.

The NAA-based sensor's surfaces after the displacement assays were also analyzed by scanning electron microscopy and their atomic composition was determined by EDXS analysis. The results obtained for sensor **S1** are shown in **Figure 5** and **Table 4**. A surface morphology with more opened porous structure can be seen in the image of sensor incubated with the complementary oligonucleotide **O3-S1C**. Moreover, P, C, N, and O atomic content is lower than that for the corresponding control sensor, supporting the above-mentioned transduction mechanism involving the displacement of the capping oligonucleotide **O2-S1** in the presence of the complementary **O3-S1C**.

In a further step, the validation of the nine sensors for the detection of 14 different hr-HPV types in 43 clinical samples of patients from Hospital Universitari i Politècnic La Fe, was carried out. Vaginal material was collected from cervical scrapes for both accurate cytological assessment and HPV testing. DNA testing of hr-HPV types was done using multiplex real-time PCR assays
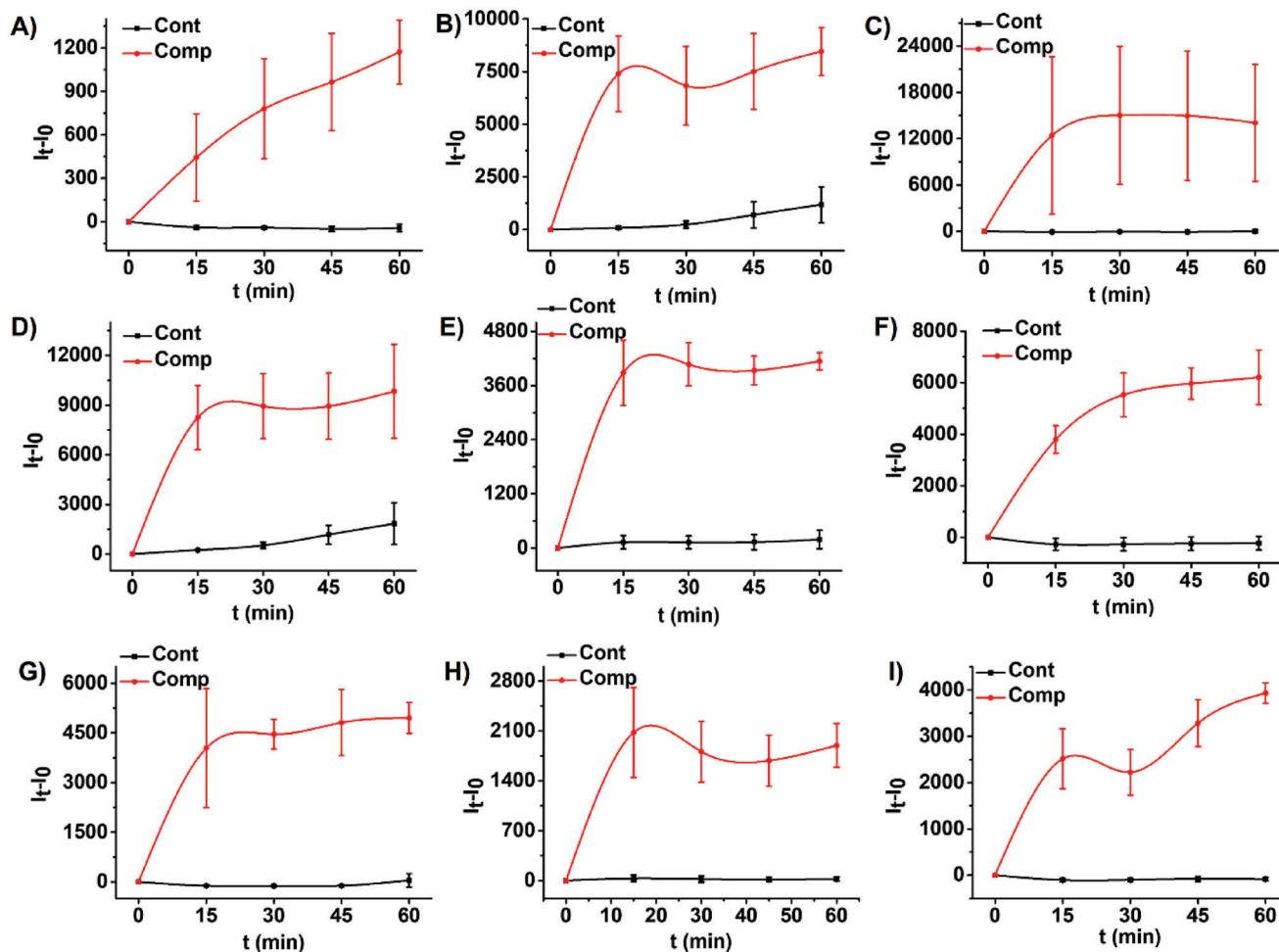
**ADVANCED
SCIENCE NEWS**

www.advancedsciencenews.com

**ADVANCED
HEALTHCARE
MATERIALS**

www.advhealthmat.de

Figure 4. Rhodamine B release profiles from the 9 sensors (**S1** A); **S2** B); **S3** C); **S4** D); **S5** E); **S6** F); **S7** G); **S8** H), and **S9** I)) incubated (Comp) or not (Cont) with the corresponding complementary oligonucleotides **O3-S1C-9C**.
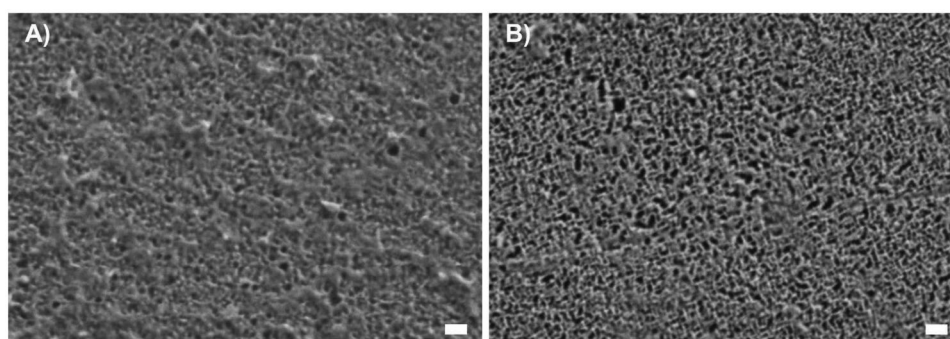

Figure 5. HR-FESEM images of NAA based sensor's surface (**S1**) after incubation with TRIS A) and complementary oligonucleotides **O3-S1C** B) (Scale bars: 100 nm).

(Cobas 4800 HPV test and Seegene ANYPLEX II HPV28 detection kit) for detection and identification of 14 hr-HPV (types 16, 18, 31, 33, 35, 39, 45, 51, 52, 56, 58, 59, 66, and 68). Data of clinical samples were summarized in **Table 5** and Table S15 (Supporting Information). At the same time, detection of HPV in vaginal materials was also carried out using sensors **S1-9**.

All **S1-9** NAA sensors were incubated with the 43 vaginal samples collected in PreservCyt medium and released RhB was measured by fluorescence spectroscopy. Data of fluorescence intensity variations at 15 min respect to initial intensity ($I_{15}-I_0$) for each sensor is plotted as scatter dispersion chart, and a box chart representing data distribution is also drawn (**Figure 6**). For instance,
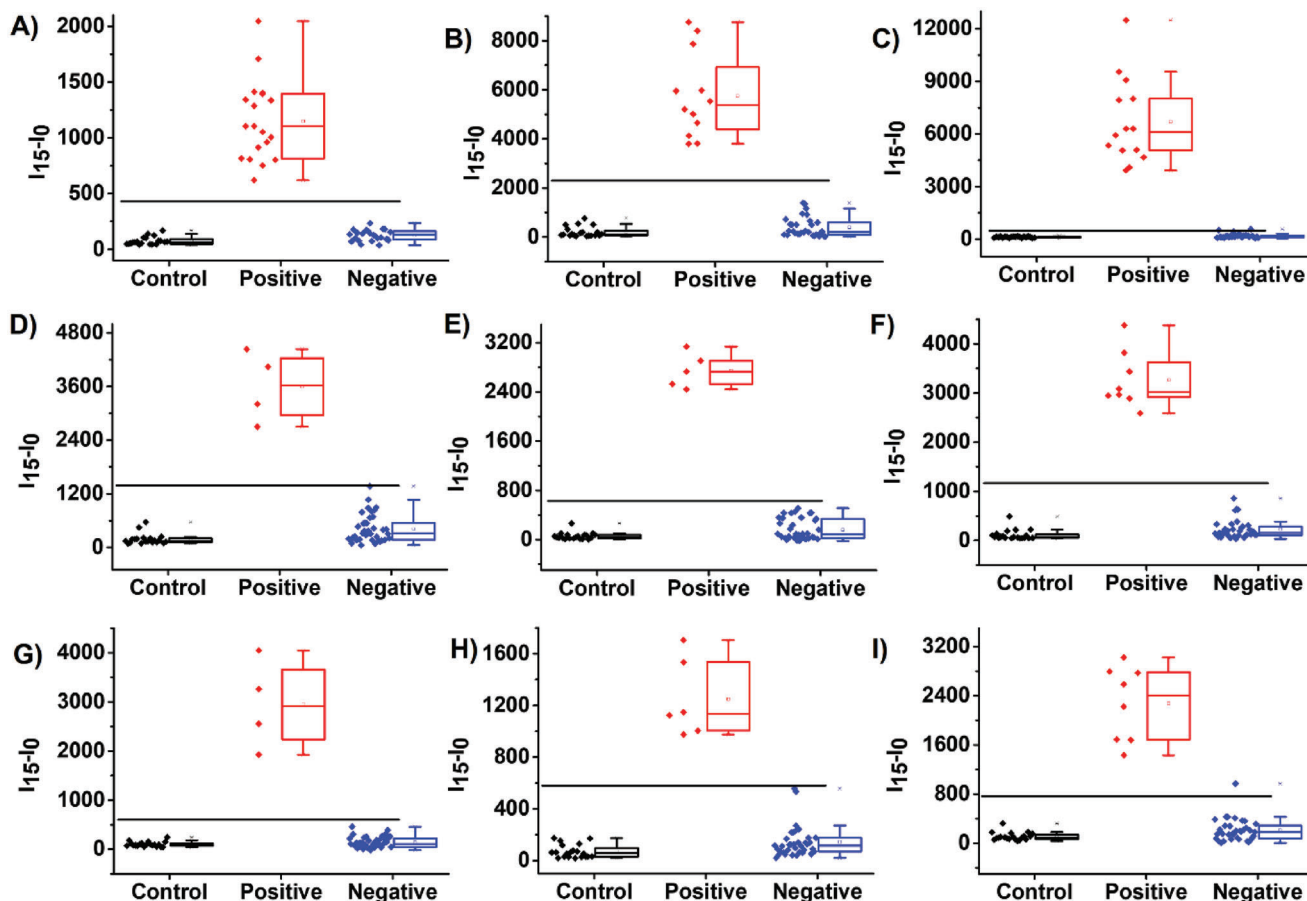
**ADVANCED
SCIENCE NEWS**

www.advancedsciencenews.com

**ADVANCED
HEALTHCARE
MATERIALS**

www.advhealthmat.de

Figure 6. Detection of different hr-HPV types in 43 clinical samples using the 9 sensors developed (**S1** A); **S2** B); **S3** C); **S4** D); **S5** E); **S6** F); **S7** G); **S8** H), and **S9** I)).

Table 5. Data of clinical samples of patients from Hospital Universitari i Politècnic La Fe.

Patient ages (years)	<30	30–39	40–49	>49
	6	15	12	9
HPV type	16	18	Others	
	9	10	28	
Cytological Result *	Negat	LSIL	HSIL	ASCUS
	26	11	1	5

*Negat: Negative; LSIL: Low grade squamous intraepithelial lesion; HSIL: High grade squamous intraepithelial lesion; ASCUS: Atypical squamous cells of undetermined significance

the obtained results for sensor **S1** (able to detect HPV types 16, 18, and 59) are shown in Figure 6A. The signal of the **S1** sensors incubated with samples containing at least one of the 16, 18, and 59 HPV types (as determined by multiplex real-time PCR assays, *vide ante*) was plotted as red squares (labeled as positive, 19 samples). On the other hand, data for **S1** sensors incubated with samples that do not contain 16, 18, and 59 HPV types, were plotted

as blue squares (labeled as negative, 24 samples). Note that more than one of those types, and even other types, are present in some of those samples. The signal threshold (horizontal straight line) to decide which samples are positives and negatives using the sensing assay with **S1**, was established at the signal mean plus ten times the standard deviation for 20 **S1** sensors (black squares) incubated with PreservCyt medium and labeled as control sensors. Following this decision criteria, for sensor **S1**, 19 samples were classified as positives (True positives: 19 and False positives: 0) for at least one of the HPV types 16, 18, or 59; whereas 24 samples were classified as negatives (True negatives: 24 and False negatives: 0) (**Table 6**). As it has been described previously the stepwise transduction mechanism in these gated porous support-based sensors implies two spatiotemporally separated events: a recognition step of the target analyte (pathogen´s DNA) by the gatekeeper on the external surface, and the further signaling event involving the release of high amount of the reporter molecules (RhB) from pores. A signal amplification, instead of analyte amplification using PCR based assays, is an advantage of these gated sensors for highly sensitive DNA detection.[32,36]

Similar studies were also carried out with the remaining **S2-9** sensors and results are plotted in Figure 6B–I and in Table 6. Very high sensitivity, negative predictive values (100%), specificities of 93–100% and positive predictive values in the range 88–100%,

ADVANCED
SCIENCE NEWS

www.advancedsciencenews.com

ADVANCED
HEALTHCARE
MATERIALS

www.advhealthmat.de

Table 6. Validation of the 9 sensors for detection of different hr-HPV types in 43 clinical samples.

Sensor	hr-HPV type	Positive sample	Negative sample	True positive	True negative	False positive	False Negative	Sensitivity [%]	Specificity [%]	Positive predictive value [%]	Negative predictive value [%]
S1	59, 16, 18	19	24	19	24	0	0	100	100	100	100
S2	45, 18	12	31	12	31	0	0	100	100	100	100
S3	31, 16	14	29	14	27	2	0	100	93	88	100
S4	51	4	39	4	39	0	0	100	100	100	100
S5	52	5	38	5	38	0	0	100	100	100	100
S6	33, 58	8	35	8	35	0	0	100	100	100	100
S7	35, 33	4	39	4	39	0	0	100	100	100	100
S8	56, 66	6	37	6	37	0	0	100	100	100	100
S9	68, 39	8	35	8	34	1	0	100	97	89	100

were calculated. The lowest values were obtained for sensors **S3** and **S9** for detection of HPV types 16/31 and 39/68, respectively. This behavior, regarding a relatively lower specificity and positive predictive values compared to sensitivity and negative predictive values, is very common in other standard DNA detection methods for HPV infection screening in clinical samples, due to their very low limit of detection and high sensitivity that generally shows an inverse relationship respect to specificity.[20] Moreover, the receiver-operating characteristic (ROC) analysis was carried out for validation of sensors **S1-9** to discriminate between negative and positive samples (Figure S4, Supporting Information). An area under curve (AUC) of 1, sensitivity and specificity of 100% were obtained for all sensors supporting the potential of these gated porous supports as a diagnosis tool.

Sensors and sensing assays developed in this work allowed a rapid multiplexed analysis of clinical samples, enabling screening of infections caused by different hr-HPV types with high sensitivity and good specificity. More in detail, the analysis of the 43 samples evaluated with the **S1-9** sensors is summarized in **Table 7**. Samples were classified as positive (**+**) and negative (-) for the different HPV types detected using the 9 sensors developed. False positive (o) samples were also labeled. As an example, the assays on sample 1 allow to determine that the sample does not contain hr-HPV types **16, 18, 31, 39, 45, 52, 56, 59, 66**, and **68**, whereas it contain hr-HPV types **33, 35**, and/or **58**, whereas analysis for instance on sample 20 determines that it contain hr-HPV types **39** and/or **68**. Compared to other biosensors reported for HPV detection, the sensor design and detection protocol described in this work have some advantage regarding the high number of hr-HPV types that can be detected, as recently reported biosensors are designed to only detect hr-HPV types **16** and **18**.[22,23,25,28] Besides, our work demonstrates that a fast and accurate detection of 14 different hr-HPV types in clinical samples can be achieved, whereas for other biosensors previously described HPV detection in clinical samples is usually not reported.[24,26,27,29] The sensing assays reported in this work allow to carry out a multiplexed analysis of clinical samples using an integrated platform for analyte recognition, transduction, and signal reading, allowing faster screening of samples which can be carried out by non-specialized personnel.

3. Conclusion

Nine sensors based on oligonucleotide gated NAA films loaded with RhB as fluorogenic reporter, are developed for the rapid and sensitive detection of 14 different types of HPV. The preparation protocol is optimized to scale up the production of sensors in a reproducible manner. Key experimental tips are related to using a gentle stirring with an orbital stirrer and controlling the humidity during the external surface modification of the nanoporous materials. Sensors are characterized by scanning electron microscopy and the atomic composition of the surfaces was determined after each functionalization step by EDXS. The increase of atomic ratio between C, O, N, Si, and P respect to Al confirm the modification of NAA surface with the alkoxysilane, the oligonucleotide **O1** and the different capping oligonucleotides **O2-S1-9**. The capacity of the sensors to selectively detect the oligonucleotides **O3-S1C-9C** complementary to capping oligonucleotides **O2-S1-9** is confirmed by fluorescence measurements. Only, when the complementary oligonucleotides **O3-S1C-9C** is present in the medium a remarkable RhB release from nanoporous materials is observed. Finally, the sensors are used for the sensitive detection of 14 different types of HPV in 43 clinical samples. High sensitivity and negative predictive values (100% for both) are observed for all sensors. Also, high specificity and positive predictive values are found.

4. Experimental Section

Materials: Nanoporous anodic alumina films on Al foils (25 × 75 mm) were purchased from InRedox (Alumina thickness: 10 ± 0.2 μm; pore diameter: 5 ± 2 nm, pore density: 9×10^{11} cm^{-2}, porosity: 15 ± 2%). Oligonucleotides were purchased from Integrated DNA Technologies (IDT). Sequences of the 19 oligonucleotides used for sensor synthesis and sensing assay were listed in Table 1. Rhodamine B, 3-(triethoxysilyl)propyl isocyanate, triethylamine, acetonitrile (anhydrous), tris(hydroxymethyl)aminomethane (TRIS), magnesium chloride (anhydrous), and hydrochloric acid were purchased from Sigma Aldrich.

Table 7. Multiplexed analysis of 43 clinical samples for screening infections caused by 14 different hr-HPV types using the 9 NAA based sensors developed.

Sample	hr-HPV type*	S1** (59, 16, 18)	S2 (45, 18)	S3 (31, 16)	S4 (51)	S5 (52)	S6 (33, 58)	S7 (35, 33)	S8 (56, 66)	S9 (68, 39)
1	33	-	-	-	-	-	+	+	-	-
2	33	-	-	-	-	-	+	+	-	-
3	33	-	-	-	-	-	+	+	-	O
4	35, 52	-	-	-	-	+	-	+	-	-
5	39	-	-	-	-	-	-	-	-	+
6	39, 51	-	-	-	+	-	-	-	-	+
7	45	-	+	-	-	-	-	-	-	-
8	45, 58	-	+	-	-	-	+	-	-	-
9	51	-	-	-	+	-	-	-	-	-
10	51, 58	-	-	-	+	-	+	-	-	-
11	51, 58	-	-	-	+	-	+	-	-	-
12	52	-	-	-	-	+	-	-	-	-
13	52, 68	-	-	-	-	+	-	-	-	+
14	52, 68	-	-	-	-	+	-	-	-	+
15	56	-	-	-	-	-	-	-	+	-
16	58	-	-	-	-	-	+	-	-	-
17	58	-	-	-	-	-	+	-	-	-
18	59	+	-	-	-	-	-	-	-	-
19	66	-	-	o	-	-	-	-	+	-
20	68	-	-	-	-	-	-	-	-	+
21	16	+	-	+	-	-	-	-	-	-
22	16	+	-	+	-	-	-	-	-	-
23	16	+	-	+	-	-	-	-	-	-
24	16	+	-	+	-	-	-	-	-	-
25	16	+	-	+	-	-	-	-	-	-
26	16, 31, 56	+	-	+	-	-	-	-	+	-
27	16, 39	+	-	+	-	-	-	-	-	+
28	16, 39, 52, 66	+	-	+	-	+	-	-	+	+
29	16, 18	+	+	+	-	-	-	-	-	-
30	18	+	+	-	-	-	-	-	-	-
31	18	+	+	-	-	-	-	-	-	-
32	18	+	+	-	-	-	-	-	-	-
33	18	+	+	-	-	-	-	-	-	-
34	18	+	+	-	-	-	-	-	-	-
35	18	+	+	o	-	-	-	-	-	-
36	18	+	+	-	-	-	-	-	-	-
37	18	+	+	-	-	-	-	-	-	-
38	18	+	+	-	-	-	-	-	-	-
39	31	-	-	+	-	-	-	-	-	-
40	31	-	-	+	-	-	-	-	-	-
41	31	-	-	+	-	-	-	-	-	-
42	31, 66, 68	-	-	+	-	-	-	-	+	+
43	31, 56	-	-	+	-	-	-	-	+	-

*HPV types detected using multiplex real-time PCR assays (Cobas 4800 HPV test and Seegene ANYPLEX II HPV28 detection kit) **HPV types detected using the 9 sensors developed: positive (+); negative (-); false positive (o)

Characterization Techniques: High Resolution Field Emission Scanning Electron Microscopy (HR-FESEM): NAA sensors were placed onto Al disks using carbon cement. Images were acquired using a HR-Field Emission Scanning electron microscope (ZEISS GeminiSEM 500) operating at 5 kV. The atomic composition of analyzed surfaces was determined by Energy Dispersive X-ray Spectroscopy (EDXS) using an X-ray detector coupled to microscope. Fluorescence measurements were acquired using

a Synergy H1 microplate reader (BioTek, Winooski, VT, USA). Absorption spectra were recorded using a JASCO V-650 UV/vis spectrophotometer.

Synthesis Protocol: NAA films on Al disks (diameter: 2 mm, 24 disks) were soaked in RhB solution in acetonitrile (1.5 mM, 10 mL) at 25 °C during 18 h using an orbital stirrer at 50 rpm. 3-(Triethoxysilyl)propyl isocyanate (1 mL) was added dropwise, and the mixture was stirred for 6 h. NAA disks were washed with RhB in acetonitrile (1.5 mM) and dried with paper. NAA disks (48 disks) were soaked in RhB solution in acetonitrile (1.5 mM, 5 mL), then aqueous solution of oligonucleotide O1 (Table 1) bearing an amine group (100 µM, 60 µL) and triethylamine (24 µL) were added subsequently. The mixture was stirred at 25 °C for 3 h using an orbital stirrer at 50 rpm. NAA disks were washed with RhB in acetonitrile (1.5 mM) and dried with paper. Finally, NAA disks (48 disks) were soaked in TRIS buffer (20 mM, MgCl$_2$ 37.5 mM, 5 mL) and then, an aqueous solution of capping oligonucleotides **O2-S1-9** (100 µM, 240 µL) was added. The mixture was stirred at 25 °C during 2 h using an orbital stirrer at 50 rpm. NAA disks were washed three times with TRIS buffer and dried with paper. Aliquots of supernatants after capping and washing steps were collected for absorbance and fluorescence measurements.

Sensing Assay: NAA based sensors were soaked in TRIS buffer (1 mL per sensor), then aliquots (200 µL) were taken and added to 96 well plate for initial fluorescence measurements (excitation wavelength (λ_{ex}) = 555 nm, emission wavelength (λ_{em}) = 585 nm) using a plate reader. From the 200 µL, 100 µL was discarded and then, 100 µL of water or aqueous solution of uncapping oligonucleotides **O3-S1C-9C** (1 µM, 100 µL) complementary with capping oligonucleotides **O2-S1-9** used for surface modification of NAA films (Table 1), was added. Mixtures were shaken at 25 °C using a thermoshaker at 700 rpm. At scheduled times (15, 30, 45, and 60 min) aliquots (200 µL) were taken for fluorescence measurements in the same wells than previous ones and mixed again with sensors after measurements. The assay was carried out in triplicate for the nine different sensors.

Sample Collection and HPV Detection using Reference Methods: Vaginal material was collected from cervical scrapes by clinician ensuring adequate specimen collection (sufficient ectocervical and/or endocervical cells in the cervical transformation zone) for both accurate cytological assessment and HPV testing (Table 5). Samples were stored in liquid media using PreservCyt solution from Hologic (Thin Prep 5000).

DNA testing of hr-HPV types was done using multiplex real-time PCR assays (Cobas 4800 HPV test and Seegene ANYPLEX II HPV28 detection kit) for simultaneous detection and identification of 14 hr-HPV (types 16, 18, 31, 33, 35, 39, 45, 51, 52, 56, 58, 59, 66, and 68) allowing to semiquantify the viral load, from low (+; positive within 13 to 17 PCR cycles), to intermediate (++; positive within 8 to 12 cycles), to high (+++; positive within 1 to 7 cycles). (Table S14, Supporting Information)

Validation of Sensors in Clinical Samples: Clinical samples (43) of patients from Hospital Universitari i Politècnic La Fe, were collected in PreservCyt medium containing 14 different types of hr-HPV. The validation assay was like above-described sensing assay. Control sensors (20) were soaked in TRIS buffer and after initial fluorescence measurements, 100 µL of PreservCyt medium was added. At the same time 43 sensors were soaked in TRIS buffer and after initial fluorescence measurements, 100 µL of

each sample was added. Mixtures were shaken at 25 °C using a thermoshaker at 700 rpm. Aliquots (200 µL) were taken at 15 min for fluorescence measurements in the same wells than initial one. The assay was carried out for validation of the nine different sensors.

Ethical Committee: Informed written consent was obtained from all subjects included in this work, and the study was approved by the Medicaments Research Ethics Committee – CEIm of Polytechnic and University Hospital La Fe (2018/0187).

Statistical Analysis: Statistical analysis was carried out using Origin 9 and GraphPad Prism 8 softwares. Results were considered statistically significant when *P*-value was <0.05.

Supporting Information

Supporting Information is available from the Wiley Online Library or from the author.

Conflict of Interest

The authors declare no conflict of interest.

Data Availability Statement

The data that support the findings of this study are available from the corresponding author upon reasonable request.

[1] D. Forman, C. de Martel, C. J. Lacey, I. Soerjomataram, J. Lortet-Tieulent, L. Bruni, J. Vignat, J. Ferlay, F. Bray, M. Plummer, S. Franceschi, *Vaccine* **2012**, *30*, F12.

[2] L. Koutsky, Epidemiology of genital human papillomavirus infection, *Am J Med* **1997**, *102*, 3.

[3] J. M. Crow, *Nature* **2012**, *488*, S2.

[4] M. Tommasino, *Semin. Cancer Biol.* **2014**, *26*, 13.

[5] M. Grce, M. Mravak-Stipetic, *Clin. Dermatol.* **2014**, *32*, 253.

[6] H. U. Bernard, R. D. Burk, Z. Chen, K. van Doorslaer, H. zur Hausen, E. M. de Villiers, *Virology* **2010**, *401*, 70.

[7] J. Doorbar, W. Quint, L. Banks, I. G. Bravo, M. Stoler, T. R. Broker, M. A. Stanley, *Vaccine* **2012**, *30*, F55.

[8] J. Ekstrom, L. S. Muhr, D. Bzhalava, A. Soderlund-Strand, E. Hultin, P. Nordin, B. Stenquist, J. Paoli, O. Forslund, J. Dillner, *Virology* **2013**, *447*, 300.

[9] H. z. Hausen, *Bioch. Biophys. Acta* **1996**, *1288*, F55.

[10] N. Muñoz, F. X. Bosch, S. de Sanjosé, R. Herrero, X. Castellsagué, K. V. Shah, P. J. F. Snijders, C. J. L. M. Meijer, *N. Eng. J. Med.* **2003**, *348*, 518.

[11] J. M. M. Walboomers, M. V. Jacobs, M. M. Manos, F. X. Bosch, J. A. Kummer, K. V. Shah, P. J. F. Snijder, J. Peto, C. J. L. M. Meijer, N. Muñoz, *J Pathol* **1999**, *189*, 12.

[12] C. J. Meijer, J. Berkhof, P. E. Castle, A. T. Hesselink, E. L. Franco, G. Ronco, M. Arbyn, F. X. Bosch, J. Cuzick, J. Dillner, D. A. Heideman, P. J. Snijders, *Int. J. Cancer* **2009**, *124*, 516.

[13] P. K. Chan, M. A. Picconi, T. H. Cheung, L. Giovannelli, J. S. Park, *Crit. Rev. Clin. Lab. Sci.* **2012**, *49*, 117.

[14] M. E. McLaughlin-Drubin, J. Meyers, K. Munger, *Curr. Opin. Virol.* **2012**, *2*, 459.

[15] P. J. Snijders, V. M. Verhoef, M. Arbyn, G. Ogilvie, S. Minozzi, R. Banzi, F. J. van Kemenade1, D. A. M. Heideman, C. J. L. M. Meijer, *Int. J. Cancer* **2013**, *132*, 2223.

[16] G. Ronco, J. Dillner, K. M. Elfström, S. Tunesi, P. J. F. Snijders, M. Arbyn, H. Kitchener, N. Segnan, C. Gilham, P. Giorgi-Rossi, J. Berkhof, J. Peto, C. J. L. M. Meijer, *Lancet* **2014**, *383*, 524.

[17] A. A. T. P. Brink, P. J. F. Snijders, C. J. L. M. Meijer, *Disease Markers* **2007**, *23*, 273.

[18] P. J. Snijders, D. A. Heideman, C. J. Meijer, *APMIS* **2010**, *118*, 520.

[19] M. Poljak, J. Cuzick, B. J. Kocjan, T. Iftner, J. Dillner, M. Arbyn, *Vaccine* **2012**, *30*, F100.

[20] M. Poljak, A. Ostrbenk Valencak, G. Gimpelj Domjanic, L. Xu, M. Arbyn, *Clin Microbiol. Infect.* **2020**, *26*, 1144.

[21] P. Mahmoodi, M. Fani, M. Rezayi, A. Avan, Z. Pasdar, E. Karimi, I. S. Amiri, M. Ghayour-Mobarhan, *BioFactors* **2019**, *45*, 101.

[22] X. Peng, Y. Zhang, D. Lu, Y. Guo, S. Guo, *Sens. Actuators, B* **2019**, *286*, 222.

[23] A. M. Jimenez Jimenez, A. Moulick, L. Richtera, L. Krejcova, L. Kalina, R. Datta, M. Svobodova, D. Hynek, M. Masarik, Z. Heger, V. Adam, *Sens. Actuators, B* **2018**, *258*, 295.

[24] M. Shamsipur, V. Nasirian, K. Mansouri, A. Barati, A. Veisi-Raygani, S. Kashanian, *J. Pharm. Biomed. Anal.* **2017**, *136*, 140.

[25] S. Jampasa, W. Siangproh, R. Laocharoensuk, P. Yanatatsaneejit, T. Vilaivan, O. Chailapakul, *Sens. Actuators, B* **2018**, *265*, 514.

[26] P. Teengam, W. Siangproh, A. Tuantranont, C. S. Henry, T. Vilaivan, O. Chailapakul, *Anal. Chim. Acta* **2017**, *952*, 32.

[27] A. M. Jimenez Jimenez, M. A. M. Rodrigo, V. Milosavljevic, S. Krizkova, P. Kopel, Z. Heger, V. Adam, *Sens. Actuators, B* **2017**, *240*, 503.

[28] L. F. Urrego, D. I. Lopez, K. A. Ramirez, C. Ramirez, J. F. Osma, *Sens. Actuators, B* **2015**, *207*, 97.

[29] F. Chekin, K. Bagga, P. Subramanian, R. Jijie, S. K. Singh, S. Kurungot, R. Boukherroub, S. Szunerits, *Sens. Actuators, B* **2018**, *262*, 991.

[30] L. Pascual, I. Baroja, E. Aznar, F. Sancenón, M. D. Marcos, J. R. Murguía, P. Amorós, K. Rurack, R. Martínez-Máñez, *Chem. Commun.* **2015**, *51*, 1414.

[31] L. Pla, E. Xifre-Perez, A. Ribes, E. Aznar, M. D. Marcos, L. F. Marsal, R. Martinez-Máñez, F. Sancenón, *ChemPlusChem* **2017**, *82*, 337.

[32] A. Ribes, E. Aznar, S. Santiago-Felipe, E. Xifre-Perez, M. A. Tormo-Mas, J. Peman, L. F. Marsal, R. Martínez-Máñez, *ACS Sens.* **2019**, *4*, 1291.

[33] E. Aznar, M. Oroval, L. Pascual, J. R. Murguia, R. Martínez-Máñez, F. Sancenón, *Chem. Rev.* **2016**, *116*, 561.

[34] A. García-Fernández, E. Aznar, R. Martínez-Máñez, F. Sancenón, *Small* **2020**, *16*, 1902242.

[35] A. Llopis-Lorente, B. Lozano-Torres, A. Bernardos, R. Martínez-Máñez, F. Sancenón, *J. Mater. Chem. B* **2017**, *5*, 3069.

[36] F. Sancenon, L. Pascual, M. Oroval, E. Aznar, R. Martínez-Máñez, *ChemistryOpen* **2015**, *4*, 418.

[37] E. Climent, R. Martínez-Máñez, F. Sancenón, M. D. Marcos, J. Soto, A. Maquieira, P. Amorós, *Angew. Chem., Int. Ed.* **2010**, *49*, 7281.

[38] R. R. Castillo, A. Baeza, M. Vallet-Regi, *Biomater. Sci.* **2017**, *5*, 353.

[39] L. Pla, B. Lozano-Torres, R. Martínez-Máñez, F. Sancenon, J. V. Ros-Lis, *Sensors (Basel)* **2019**, *19*, 5138.

[40] A. Santos, T. Kumeria, D. Losic, *Materials (Basel)* **2014**, *7*, 4297.

[41] G. Rajeev, B. Prieto Simon, L. F. Marsal, N. H. Voelcker, *Adv. Healthcare Mater.* **2018**, *7*, 1700904.

[42] S. Alberti, G. J. A. A. Soler-Illi, O. Azzaroni, *Chem. Commun.* **2015**, *51*, 6050.

[43] W. Lee, S. J. Park, *Chem. Rev.* **2014**, *114*, 7487.

[44] W. W. Ye, J. Y. Shi, C. Y. Chan, Y. Zhang, M. Yang, *Sens. Actuators, B* **2014**, *193*, 877.

[45] W. Ye, Y. Xu, L. Zheng, Y. Zhang, M. Yang, P. Sun, *Sensors* **2016**, *16*, 1767.

[46] W. W. Ye, J. Y. Shi, C. Y. Chan, Y. Zhang, M. Yang, *Sens. Actuators, B* **2016**, *225*, 312.

[47] E. Climent, L. Mondragón, R. Martínez-Máñez, F. Sancenón, M. D. Marcos, J. R. Murguía, P. Amorós, K. Rurack, E. Pérez-Payá, *Angew. Chem., Int. Ed.* **2013**, *52*, 8938.

[48] L. Pla, S. Santiago-Felipe, M. A. Tormo-Mas, A. Ruiz-Gaitan, J. Peman, E. Valentin, F. Sancenón, E. Aznar, R. Martínez-Máñez, *Emerg Microbes Infect* **2021**, *10*, 407.

[49] L. Pla, S. Santiago-Felipe, M. Á. Tormo-Mas, J. Pemán, F. Sancenón, E. Aznar, R. Martínez-Máñez, *Sens. Actuators, B* **2020**, *320*, 128281.

[50] L. Pla, A. Avino, R. Eritja, A. Ruiz-Gaitan, J. Peman, V. Friaza, E. J. Calderon, E. Aznar, R. Martínez-Máñez, S. Santiago-Felipe, *J Fungi (Basel)* **2020**, *6*, 292.

[51] I. Caballos, M. N. Aranda, A. López-Palacios, L. Pla, S. Santiago-Felipe, A. Hernández-Montoto, M. Á. Tormo-Mas, J. Pemán, M. D. Gómez-Ruiz, E. Calabuig, B. Sánchez-Sendra, C. Francés-Gómez, R. Geller, E. Aznar, R. Martínez-Máñez, *Adv. Mater. Technol.* **2023**, *8*, 2201913.